DOI 10.1007/s11595-016-1438-0

Hydrothermal Synthesis of WO_3 Nanowires in the Presence of Guanidine Sulfate and Its Photocatalytic Activity

MU Wanjun, YU Qianhong, LI Xingliang, WEI Hongyuan, JIAN Yuan*
(Institute of Nuclear Physics and Chemistry, China Academy of Engineering Physics, Mianyang 621900, China)

Abstract: WO_3 nanowires were fabricated by a hydrothermal method, which proceeded at 170 ℃ for 48 h in a solution containing $C_2H_{10}N_6H_2SO_4$ as a dispersant and Na_2WO_4 as a starting material. The nanowires exhibit a well crystallized one-dimensional structure with 20 nm in diameter and several microns in length. The physicochemical properties of WO_3 were compared using X-ray diffraction (XRD), scanning electron microscopy (SEM), transmission electron microscopy (TEM), energy dispersive X-ray spectroscopy (EDX) and UV-vis spectroscopy (UV-Vis). The photoactivity of the as-perpared WO_3 nanowires was evaluated through the photodegradation of methylene blue (MB) in aqueous solution. The experimental results demonstrate that addition of $C_2H_{10}N_6H_2SO_4$ salt in the WO_3 nanowires synthesis process can enhance its photocatalytic activity obviously.

Key words: hydrothermal method; WO_3 nanowires; crystal structure; photocatalytic

1 Introduction

Recently, one-dimensional(1D) nanostructure such as nanorods, nanobelts, nanowires and nanotubes have attracted remarkable interest due to their novel physical and chemical properties as well as their potential applications in chemistry of nanomaterials[1]. As a prominent example, 1D tungsten oxides, because of their lower dimensionality and superior properties, have been widely applied in semiconductor gas devices[2], electrochromic devices[3], and photocatalysts[4]. Especially, hexagonal tungsten trioxide (*hex*-WO_3) has been considered as an intercalation host for obtaining hexagonal tungsten bronzes $MxWO_3$ ($M=Li^+$, Na^+, K^+, *etc*)[5], and as a promising electrocatalyst for hydrogen evolution reactions[5].

Tungsten oxide nanowires or nanorods were synthesized by heat treatment of tungsten metal; such as a tungsten wire partly wrapped with boron oxide in nitrogen atmosphere at 1600 ℃, an electrochemical etched tungsten at 700 ℃ in an Ar atmosphere, and a tungsten foil partly covered by SiO_2 plate in an argon atmosphere at 1600 ℃[6,7]. Recently, the hydrothermal synthesis of ultralong and single crystalline $Cd(OH)_2$ nanowires using alkali salts as mineralizers was reported by Tang *et al*[8]. The 1D nanostructure synthesis using inorganic salt instead of surfactant and water-soluble high molecule has strongpoints in non-pollution, low-cost, easy-cleanout and recovery. Simultaneously, the hydrothermal method has been proved to be a powerful tool to synthesize anisotropic nanomaterials with significant advantages, such as controllable particle size, low-temperature, cost-effectiveness, and simple operation[9-12]. In this study, we report a facile inorganic route for the synthesis of hex-WO_3 nanowires without use of any templates and surfactants in aqueous solution. The morphology of WO_3 was controlled by addition of different content of guanidine sulfate salt ($C_2H_{10}N_6{\cdot}H_2SO_4$). In addition, the photocatalytic activities of the as-prepared samples for the methylene blue (MB) photodegradation were investigated.

2 Experimental

2.1 Synthesis procedure

All chemicals used were purchased without

(Received: Apr. 20, 2015; Accepted: June 11, 2015)
MU Wanjun(牟婉君): E-mail:jun19820922@163.com
* Corresponding author: JIAN Yuan (蹇源): Prof.; E-mail: inpc207@163.com
Funded by the National Natural Science Foundation of China (No.21501159)

further dealing with unless otherwise specified.

To synthesize 1D WO_3, 2 g $Na_2WO_4{\cdot}2H_2O$ was dissolved in 45 mL deionized water under stirring at room temperature and 5 mL of 3 $mol{\cdot}L^{-1}$ HCl solution was added dropwise into the above solution under continuous stirring. Then $C_2H_{10}N_6{\cdot}H_2SO_4$ was added in this suspension, followed by transferring into a Teflon-lined autoclave, in which the solution was allowed to remain at 170 ℃ for 48 h. After that, the autoclave cooled down naturally. The finally products were collected by glasswares, then washed with deionized water and ethanol three times, and then dried in air at 80 ℃. The WO_3 nanowires were finally obtained.

2.2 Materials analysis

The crystallinity of WO_3 nanostructures was characterized using an X-ray diffractometer (PXRD, X'Pert PRO, PANalytical, Almelo, Netherlands) with Cu-Ka radiation (λ=0.15406 nm at 40 kV and 45 mA). The sizes and shapes of the nanostructures were observed on a field emission scanning electron microscope (FE-SEM Philips XL30 FEG, Eindhoven, Netherlands) and a transmission electron microscopy (TEM, JEM200CX, 120 kV).The composition of the product was analyzed by an energy dispersive X-ray detector (EDX, Thermo Noran VANTAG-ESI, 120 kV). UV-vis diffuse reflectance spectroscopy was carried out on a UV-vis spectrophotometer (Lambda 850, PerkinElmer, USA), equipped with an integrating sphere and a $BaSO_4$ reference.

2.3 Photocatalytic experiments

Photocatalytic activities of the photocatalyst samples were evaluated by observing the degradation of the MB aqueous solution at ambient temperature using a 300 W high-pressure mercury lamp as light source. In a typical process, 50 mg of photocatalyst was added to 100 mL of 10 mg/L MB aqueous solution in a quartz glass container. Prior to irradiation, the solution was continuously stirred in the dark for 1 h to ensure the equilibrium of the working solution. The suspensions were kept under constant air-equilibrated conditions before and during the irradiation. Analytical samples (3 mL) were drawn from the reaction suspension every 10 min and after removal of the photocatalyst by centrifugation, the concentration of residual MB aqueous solution was measured by the UV-vis spectrophotometer at 550 nm.

3 Results and discussion

The overall morphology of the sample is shown in Figs.1(a)-1(c). It is clearly indicated from these images that the WO_3 nanowire had been synthesized. The proportion of the nanowire morphology was estimated to be about 95% (Fig.1(a)). The average diameters of these uniform nanowires were about 30 nm(Fig.1(c)) and the length was up to several microns (Fig.1(b)). The energy dispersive spectrometric (EDS) analysis was employed to analyze the composition of the tungsten oxide nanowires. As shown in Fig.2(a), only oxygen and tungsten elements existed in the nanowires with molar ratio of about 3 (O/W). The XRD pattern of tungsten oxide nanowire is shown in Fig.2(b), which can be indexed undisputedly to hexagonal WO_3 (with the XRD pattern corresponding to JCPDS card 35-1001). The XRD peak intensity of the [001] plane is stronger compared with that of other planes, indicating that the [001] is the major growth direction.

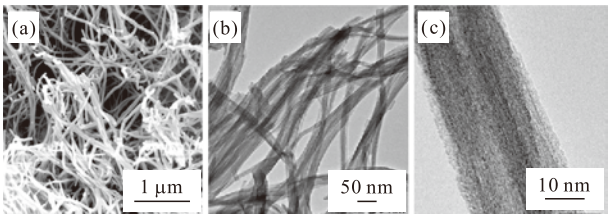

Fig.1 Images of WO_3 nanowires synthesized at 170 ℃ for 48 h with 4 g $C_2H_{10}N_6{\cdot}H_2SO_4$: (a)SEM; (b)TEM; (c)TEM

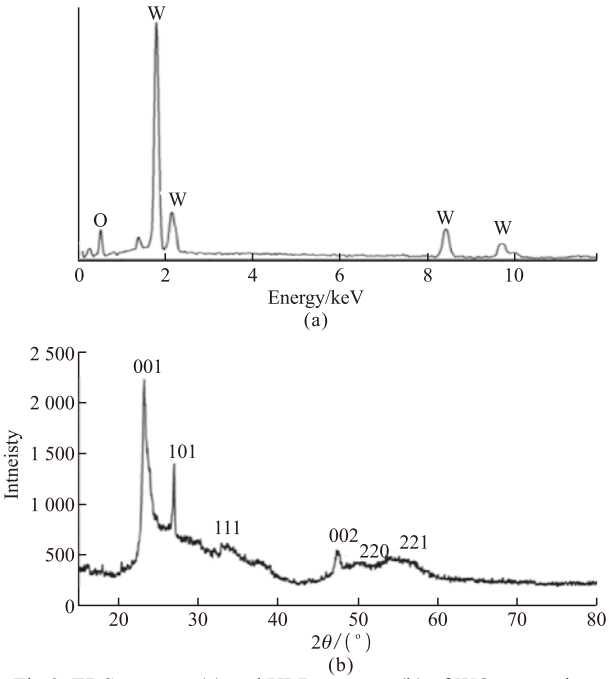

Fig.2 EDS patterns (a) and XRD patterns (b) of WO_3 nanowires

The addition content of $C_2H_{10}N_6{\cdot}H_2SO_4$ would affect the morphologies and dimensions of the WO_3 in the same hydrothermal system, different amount of $C_2H_{10}N_6{\cdot}H_2SO_4$ was studied. The SEM

images of the samples are shown in Figs.3(a)-3(c). As shown in Fig.3(a), the sample with the addition of 1g $C_2H_{10}N_6{\cdot}H_2SO_4$ exhibits a matrix structure of nanosheets. With the additions of 2 g and 3 g $C_2H_{10}N_6{\cdot}H_2SO_4$, the morphologies of synthesized WO_3 (Figs.3(b) and 3(c)) are the meshy structure of nanowires. When the content of $C_2H_{10}N_6{\cdot}H_2SO_4$ is enhanced to 4 g, the SEM image in Figure 4d shows that nanowires with lengths around several micrometers and diameter of about 30 nm are the major products. According to these results, it can be speculated that the content of $C_2H_{10}N_6{\cdot}H_2SO_4$ plays an important role in controlling the morphologies of WO_3. To achieve a high purity synthesis of the nanowires, high proportional content of $C_2H_{10}N_6{\cdot}H_2SO_4$ is needed. To further insight into the temperature effect, the synthesis of WO_3 with the addition of 4g $C_2H_{10}N_6{\cdot}H_2SO_4$ was also carried out at 200 ℃. It was found that the morphology has no appreciable change relative to the sample obtained at 170 ℃.

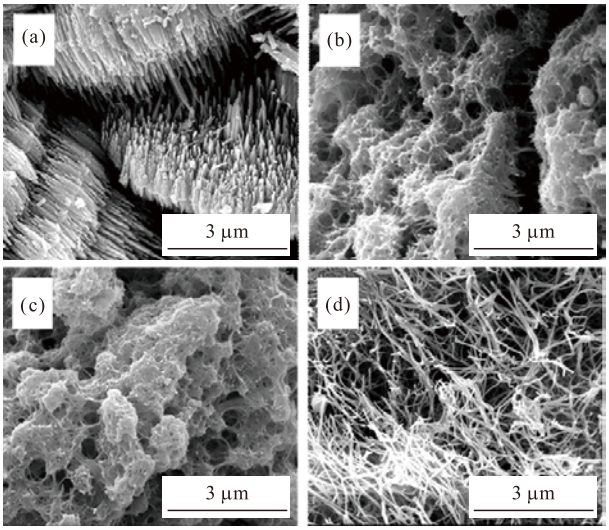

Fig.3 SEM images of WO_3 synthesized at 170 ℃ for 48 h with different amounts of $C_2H_{10}N_6{\cdot}H_2SO_4$: (a)1 g; (b) 2 g; (c) 3 g; (4) 4 g

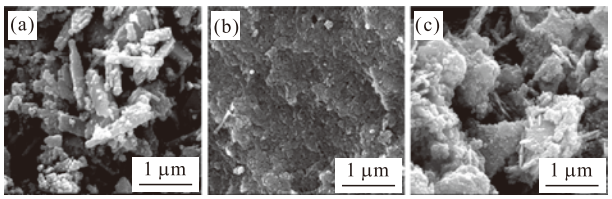

Fig.4 SEM images of WO_3 nanocrystals synthesized with different salts: (a) CH_5N_3HCl; (b) $C_2H_{10}N_6H_2CO_3$; (c) $C_2H_6N_4S$

In addition, we have carried out analogous experiments with different inorganic salts for comparison. Fig.4 displays SEM images of the obtained WO_3 with the addition of CH_5N_3HCl, $C_2H_{10}N_6H_2CO_3$, and $C_2H_6N_4S$. It is shown that no WO_3 nanowires could be obtained with given content of CH_5N_3HCl, $C_2H_{10}N_6H_2CO_3$, and $C_2H_6N_4S$. The nanorods and nanopaticles were obtained for CH_5N_3HCl and $C_2H_{10}N_6H_2CO_3/C_2H_6N_4S$, respectively. It could be concluded from the results that $C_2H_{10}N_6{\cdot}H_2SO_4$ is indispensable in the synthesis of WO_3 nanowires.

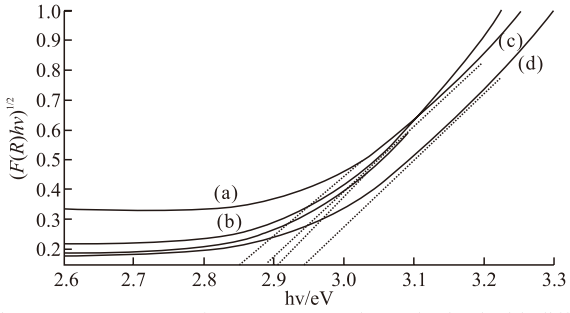

Fig.5 XRD patterens of WO_3 nanocrystals synthesized with different salts :(a) $CH_5N_3{\cdot}HCl$; (b) $C_2H_{10}N_6H_2CO_3$; (c) $C_2H_6N_4S$; (d) $C_2H_{10}N_6{\cdot}H_2SO_4$

The XRD patterns for synthesized WO_3 with various inorganic salts are compared in Fig.5. It is obviously shown that the crystalline phases for WO_3 nanocrystals are discriminatory under different conditions. According to the result, hex-WO_3 (JCPDS card 33-1387) was obtained in the presence of CH_5N_3HCl, $C_2H_{10}N_6H_2CO_3$, and $C_2H_6N_4S$. (in Figs.5(a)-5(c)). Among them, the intensities for the diffraction peaks follow the order:CH_5N_3HCl, $C_2H_{10}N_6H_2CO_3$,$C_2H_6N_4S$. On the other hand, Fig.5(d) exhibits the hexagonal reflections (JCPDS card 35-1001) in the presence of $C_2H_{10}N_6{\cdot}H_2SO_4$. Combined with the SEM results, it could be concluded that the inorganic salts had a significant effect on the crystalline phase and the corresponding morphology of WO_3. The morphologies and dimensions of synthesized nanocrystals were not only controlled by the inner structure, but also affected by the surrounding conditions such as temperature, pressure, and composition of the solution. The formation of nanowires first needs anisotropy during the growth process for the nanoparticles.

Room temperature UV-vis diffuse reflectance spectra of undoped WO_3 and Nb-doped WO_3 are shown in Fig.4. The significant increases in absorbance at wavelength shorter than 500 nm should be assigned to the intrinsic band gap absorption of tungsten oxide. Compared to undoped WO_3 nanowires, there are slightly red-shifts in the optical absorption edges for the Nb-doped . The band gap (E_g) of semiconductor can be determined according to the equation[13]:

$$(hva)^{1/n} = A(hv - E_g) \quad (1)$$

where, h, v, a, E_g, and A are the Planck's constant, the frequency of vibration, the absorption coefficient, the band gap and proportional constant, respectively. The value of the exponent n denotes the nature of the sample transition. It is known that the WO_3 crystal is an indirect allowed transition semiconductor. In this case, n=2 is used. The a in the Tauc equation can be substituted with $F(R)$. $F(R)$ is the so-called remission or Kubelka-Munk funtion[14].

$$F(R)=\frac{(1-R)^2}{2R} \quad (2)$$

where, R is the reflectance coefficient. Thus, in the actual experiment, the relational expression becomes the linear extrapolation of the plots of $(F(R)hv)^{1/2}$ *vs* hv in Fig.6. The values of the band gaps are 2.85, 2.89, 2.91, and 2.94 eV, respectively. The band gap of WO_3 is narrowed due to adding the different dispersants in reaction system.

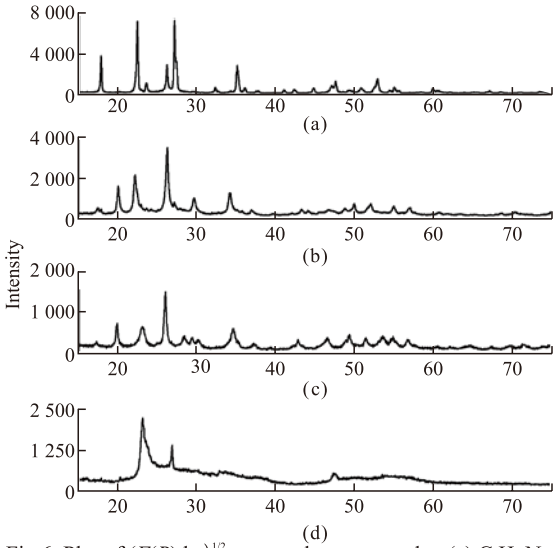

Fig.6 Plot of $(F(R)\ hv)^{1/2}$ versus photo energy hv: (a) $C_2H_{10}N_6 \cdot H_2SO_4$; (b)$CH_5N_3 \cdot HCl$; (c) $C_2H_{10}N_6H_2CO_3$; (d) $C_2H_6N_4S$

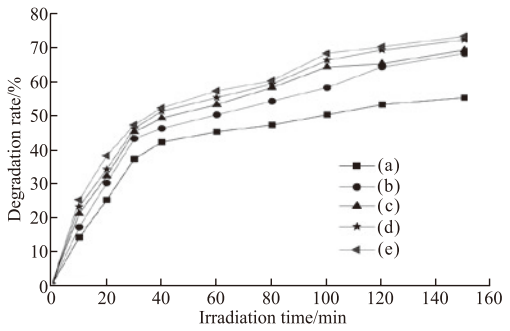

Fig.7 Photocatalytic degradation of MB by the WO_3 sample: (a) Commercial WO_3; (b-e) WO_3 prepared with different amounts of $C_2H_{10}N_6 \cdot H_2SO_4$. Here, (b)1 g; (c) 2 g; (d) 3 g; (e) 4 g

It is known that the optical properties of oxide semiconductors are directly related to their crystallinity and morphology. In this paper, the presence of K_2SO_4 is an important factor influencing the crystallization process and the growth morphology of WO_3, and further affecting optical band edge of WO_3 crystals, which leads to the formation of localized states in the band gap of WO_3, finally influencing its photocatalytic activity.

The photocatalytic activity of the as-prepared WO_3 nanowires was evaluated by the photocatalytic degradation of MB aqueous solution at ambient temperature. For comparison, the photocatalytic activities of the commercial WO_3 (sample a) and the as-prepared WO_3 nanowire (sample b-e) were also tested. Fig.7 shows the comparison of photocatalytic activity of the various WO_3 photocatalysts. It can be seen that the concentration of $C_2H_{10}N_6 \cdot H_2SO_4$ has a significant effect on the photocatalytic activity of the as-prepared samples. The sample E showed the highest photocatalytic activity due to its good dispersion in the reaction solution. Moreover, the beautiful morphology of WO_3 nanowires was also beneficial to the enhanced photocatalytic activity. In contrast, the commercial WO_3 showed the lowest photocatalytic activity in the same irradiation time. This result clearly indicates that the addition of $C_2H_{10}N_6 \cdot H_2SO_4$ can effectively improve the photocatalytic activities. When the $C_2H_{10}N_6 \cdot H_2SO_4$ content is lower than 4 g, it is seen from Fig.7 that with increasing content, the $C_2H_{10}N_6 \cdot H_2SO_4$ degradation rate increases. With further increasing $C_2H_{10}N_6 \cdot H_2SO_4$ content, WO_3 nanowires disappear and the phtotcatalytic activity of WO_3 decreases obviously. This indicates that the crystal phase and morphologies are the vital factors that affect the photocatalytic activity of the materials. In this experiment, the presence of $C_2H_{10}N_6 \cdot H_2SO_4$ is an important factor influencing the crystallization process and the growth of the WO_3 nanowires, which controlls the rate and amount of releasing SO_4^{2-} and further affects the crystal phase, morphologies and crystallization of the WO_3 nanocrystals.

4 Conclusions

In summary, we report a simple hydrothermal method to synthesize *hex*-WO_3 nanowires with relatively uniform diameters ranging from 20 to 30 nm and lengths up to several micrometers. The concentration and composition of inorganic salt played an important role in controlling the shape

and dimensions of WO_3 nanowires. With addition of different dispersants in hydrothermal process, the WO_3 nanowires exhibited higher photocatalytic activity for the decomposition of the aqueous MB than the common WO_3. At an optimal content of $C_2H_{10}N_6{\cdot}H_2SO_4$ of 4 g, sample has the highest photocatlytic activity, the degradation rate of MB reached 72%.

References

[1] Xie G, Yu J, Chen X, *et al*. Gas Sensing Characteristics of WO_3 Vacuum Deposited Thin Films[J]. *Sens Actuators B*, 2007,123: 909-912

[2] Ashraf S, Blackman CS, Palgrave RG, *et al.* Aerosol Assisted Chemical Vapour Deposition of WO_3 Thin Films from Tungsten Hexacarbonyl and Their Gas Sensing Properties[J]. *J. Mater Chem*, 2007, 17: 3 708-3 712

[3] Xia H, Wang Y, Kong F, *et al.* Au-doped WO_3-based Sensor for NO_2 Detection at Low Operating Temperature[J]. *Sens. Actuators B*, 2008, 134: 133-139

[4] Cao B, Chen J, Tang X, *et al.* Growth of Monoclinic WO_3 Nanowire Array for Highly Selective NO_2 Detection[J]. *J. Mater. Chem.,* 2009, 19: 2 323-2 327

[5] Gu ZJ, Li HQ, Zhai TQ, *et al.* Large-scale Synthesis of Single-crystal Hexagonal Tungsten Trioxide Nanowires and Electrochemical Lithium Intercalation Intothe Nanocrystals[J]. *Journal of Solid State Chemistry*, 2007,180: 98-103.

[6] Song XC, Zheng YF, Wang Y. Large-scale Hydrothermal Synthesis of WO_3 Nanowires in the Presence of K_2SO_4[J]. *Materials Letters*, 2007, 61: 3 904-3 906

[7] Wang CK, Sahu D, Wang SC, *et al*. Electrochromic Nb-doped WO_3 Films: Effects of Post Annealing[J]. *Ceramics International*, 2012, 38: 2 829-2 834

[8] Szilagyi IM, Madarasz J, Pokol G, *et al*. Stability and Controlled Composition of Hexagonal WO_3[J]. *Chemistry of Materials*, 2008, 12: 4 116-4 121

[9] Gedanken RG. Synthesis of WO_3 Nanoparticles Using a Biopolymer as a Template for Electrocatalytic Hydrogen Evolution[J]. *Nanotechnology*, 2008, 19: 1-5

[10] Sun QJ, Xiao F, Luo JM, *et al.* Synthesis of Monodisperse $WO_3{\cdot}2H_2O$ Nanospheres by Microwave Method[J]. *Materials Letters*, 2008, 62: 2 992-2 994

[11] Liu HJ, Peng TY, Ke DN. Preparation and Potocatalytic Activity of Dysprosium Dopedtungsten Trioxide Nanoparticles[J]. *Materials Chemistry and Physics*, 2007, 104: 377-382

[12] Nimittrakoolchai OU, Supothina S. High-yield Precipitation Synthesis of Tungsten Oxide Platelet Particle and Its Ethylene Gas-sensing Characteristic[J]. *Materials Chemistry and Physics*, 2008, 112: 270-275

[13] Tauc J, Menth A, Wood DL. Optical and Magnetic Investigations of the Localized States in Semicoductiong Glasses[J]. *Phys. Rev. Lett*, 1970, 25: 749-753

[14] Kubelka P, Munk F. Ein Beitrag Zur Optik Der Farbanstriche[J]. *Z. Tech. Phys*., 1931, 12: 593-597